

Ultrastructural and transcriptome changes of free-living sporangial filaments in *Pyropia yezoensis* affected by light and culture density

Bangxiang He¹, Xiujun Xie¹, and Guangce Wang¹

¹Institute of Oceanology, Chinese Academy of Sciences

April 28, 2020

Abstract

In the life cycle of *Pyropia yezoensis*, sporangial filaments connect conchocelis and thallus, but the mechanisms of maturation and conchospore release of sporangial filaments are poorly understood. We found that the morphological change from vegetative growth form (hollow cells) to reproductive form (bipartite cells), and the release of conchospores from bipartite cells were all closely correlated with culture density and light intensity. Bipartite cells formed at low density (50–1,000 fragments/mL) and when stimulated by high light levels (40–100 $\mu\text{mol photons m}^{-2} \text{s}^{-1}$), but conchospore release was inhibited at such light intensities. At high densities (5,000–10,000 fragments/mL), sporangial filaments retained the hollow cell morphology and rarely formed bipartite cells. Ultrastructural observation showed that the degradation of autophagosome-like structures in vacuoles caused the typical hollow form. Transcriptome analysis indicated that adaptive responses to environmental changes, mainly autophagy, endocytosis and phosphatidylinositol metabolism, caused the morphological transformation of free-living sporangial filaments. Meanwhile, the extensive promotion of energy accumulation under high light levels promoted vegetative growth of sporangial filaments, and thus inhibited conchospore release from bipartite cells. These results provide a theoretical basis for maturation of sporangial filaments and release of conchospores in *P. yezoensis* and other related species.

Main text

Ultrastructural and transcriptome changes of free-living sporangial filaments in *Pyropia yezoensis* affected by light and culture density

Abstract

In the life cycle of *Pyropia yezoensis*, sporangial filaments connect conchocelis and thallus, but the mechanisms of maturation and conchospore release of sporangial filaments are poorly understood. We found that the morphological change from vegetative growth form (hollow cells) to reproductive form (bipartite cells), and the release of conchospores from bipartite cells were all closely correlated with culture density and light intensity. Bipartite cells formed at low density (50–1,000 fragments/mL) and when stimulated by high light levels (40–100 $\mu\text{mol photons m}^{-2} \text{s}^{-1}$), but conchospore release was inhibited at such light intensities. At high densities (5,000–10,000 fragments/mL), sporangial filaments retained the hollow cell morphology and rarely formed bipartite cells. Ultrastructural observation showed that the degradation of autophagosome-like structures in vacuoles caused the typical hollow form. Transcriptome analysis indicated that adaptive responses to environmental changes, mainly autophagy, endocytosis and phosphatidylinositol metabolism, caused the morphological transformation of free-living sporangial filaments. Meanwhile, the extensive promotion of energy accumulation under high light levels promoted vegetative growth of sporangial filaments, and thus inhibited conchospore release from bipartite cells. These results provide a theoretical basis for maturation of sporangial filaments and release of conchospores in *P. yezoensis* and other related species.

Keywords: High light, Culture density, Environmental adaptation, Nutrient limitation, Autophagy, Vegetative growth, Reproductive transformation, Transcriptome, Cell morphology

Introduction

Pyropia yezoensis, as a potential model marine species in the intertidal zone, has a strong adaptability to environmental changes (Blouin, Brodie, Grossman, Xu, & Brawley, 2011). *P. yezoensis* is cultivated in many countries including China, Japan, and Korea (Kim, Yarish, Hwang, Park, & Kim, 2017). The annual yield of *Pyropia/Porphyra* has exceeded 110,000 tons in recent years and its production shows an upward trend in China, associated with significant economic value (Ma, He, Huan, Lu, & Wang, 2019). In 1949, Drew (Drew, 1949) found that the algae “conchocelis”, which grew in shells, was a stage in the life cycle of the *Porphyra* genus. Thereafter, the complete life history of *Pyropia/Porphyra* was gradually elucidated. In nature, the macroscopic thallus (gametophyte, haploid) would form a micro conchocelis (sporophyte, diploid) through carpospores (zygote, sporophyte). The carpospores would attach to shells and develop into conchocelis, which then developed into sporangial filaments (in some studies called conchosporangium, being the late stage of conchocelis) and the matured sporangial filaments would then release conchospores (diploid) under suitable conditions. Conchospores would undergo meiosis during the first or first two cell divisions and develop into a haploid thallus again (Blouin et al., 2011; Yoji et al., 2013).

The conchocelis stage of *P. yezoensis* is more sensitive to environmental changes than gametophyte generation, because the thallus is able to survive under many stressful conditions, such as drought during daytime low tide and high light in which the conchocelis would die. In nature, the growth and maturation of the conchocelis stage in *P. yezoensis* all occur on a shell substrate, which could provide a relatively stable environment compared with free-living in the sea. Because of this, it is relatively easier to control the development and conchospore release in a shell-culture system than in a free-living system. At present, shell-culture systems remain the main method used in large-scale artificial seedling collection of *P. yezoensis*, but this method takes a long time (6–7 months), and requires huge shell consumption and large labor costs (He & Yarish, 2006). It has been shown that the conchocelis stage, consisting of sporangial filaments, can be vegetatively propagated in a free-living way (Chen, 1980; Sun & Zheng, 1996; Yang & He, 2004). There have been some efforts made to seed using free-living conchocelis and omit the long shell-culture period, but this approach is still not widely used (He & Wu, 2003). The main problem is the difficulty of consistently controlling maturation and conchospore release of free-living conchocelis or sporangial filaments.

In sporophyte generation, sporangial filaments are directly related to conchospore release. Observation has revealed that in shell-cultured sporangial filaments, when a large number of bipartite cells appeared—the typical features of which are short, round cells, which are paired and compact—massive conchospore release would follow. Bipartite cell formation is the sign of maturity in sporangial filaments. The vegetative propagation of sporangial filaments indicated that these special bipartite cells have the ability to directly develop into gametophytes when released and also to maintain the ability of vegetative growth of sporophytes when not released. Many physiological studies on sporophyte generation in *P. yezoensis* have shown that vegetative growth and conchospore release are significantly affected by the culture environment, mainly including temperature, light, photoperiod, and culture density (Chen, 1980; He & Yarish, 2006; Li, Yang, & He, 2011; López-Vivas, Riosmena-Rodríguez, Pacheco-Ruíz, & Yarish, 2015; Waaland, Dickson, & Carrier, 1987; Yang & He, 2004). However, the molecular mechanism behind sporangial filament development has rarely been studied.

In this study, we observed some interesting phenomena regarding the effects of culture density and light intensity on maturation and conchospore release of free-living sporangial filaments. Further, through observation by transmission electron microscope (TEM) and analysis of the transcriptome, the morphological characteristics and gene expression of free-living sporangial filaments were explored. We believe our findings will be helpful in increasing the in-depth understanding of the development of sporangial filaments under different environmental conditions and for application to the free-living method of seeding *Pyropia/Porphyra*.

Materials and Methods

Preservation of free-living sporangial filaments

In order to obtain pure free-living sporangial filaments, we directly selected a single clone of sporangial filament from conchocelis and through step-by-step amplification culture, eventually obtained a large number of vegetatively-propagated sporangial filaments. These sporangial filaments were preserved long-term (more than 6 months) in 23°C, 50 $\mu\text{mol photons m}^{-2} \text{s}^{-1}$ irradiance (light:dark =10:14), using PES (Provasoli, 1968) medium with 100 mg/L ampicillin and streptomycin. The medium was replaced every two weeks and the filaments were cut off the culture every three months.

Experimental conditions and setting of filament fragment densities

In order to explore maturation (a typical characteristic of which is the formation of bipartite cells) and conchospore release of sporangial filaments, we set a daily cooling system, from 21 (dark) to 18 (light) with a 10:14 (light:dark) photoperiod. In light experiments, light intensity was adjusted to 10, 20, 40, 60, 80 or 100 $\mu\text{mol photons m}^{-2} \text{s}^{-1}$ through different degrees of occlusion using white printing paper. In order to create different culture densities, moderate sporangial filaments were collected through a 70 μm cell strainer and put into a 1.5 mL Eppendorf tube and then point cut about 30–40 times at a speed of 12,000 rpm through a tissue homogenizer (Tiangen Biotech Co. Ltd., Beijing, China) and re-suspended. We then diluted the fragment suspension to an appropriate multiple and counted the number of filament fragments and then calculated the density of the original fragments in the suspension, and finally, used this calculated original fragment suspension to create a gradient of different filament fragment densities (0.5, 1, 5, 10, 50, 100 \times 100 fragments/mL) in a 48-well plate with 1 mL culture medium. Based on this method, we created a linear prediction of the relationship between filament densities and fresh weight of sporangial filaments (Suppl. Fig. 1) and used this linear equation to estimate the filament densities in the initial experiments of growth and transcriptome experiments. The proportion of bipartite cells was calculated by the random visual field method, which involved counting the number of sporangial filament fragments with bipartite cells (typical cell features were short, round, paired and compact) in the first 30 fields under 10 \times 10 magnification through an inverted microscope (Nikon, Tokyo, Japan). The count was repeated every 3 days over 15 days of culture and the experiment was repeated in triplicate.

Fresh weight measurement of sporangial filaments

In order to explore the growth changes of sporangial filaments under different light intensities, we analyzed the fresh weight of sporangial filaments under the daily cooling system every week in 4-week culture. All other conditions were the same as above except for the light intensities. Three light intensities were used, which were 10, 40, and 80 $\mu\text{mol photons m}^{-2} \text{s}^{-1}$. The initial fresh weight of sporangial filaments was set at 20 mg and they were cultured in 200 mL PES medium with kanamycin (400 mg/L) in 250 mL conical flasks, so that the filament density was approximately 1,300 fragments/mL. The fresh weight was measured every week over the 4-week culture period after they were collected and measured after as much moisture as possible was absorbed using sterilized dust-free paper. The medium was changed weekly and all groups were analyzed in triplicate.

Conchospore release by sporangial filaments

In order to explore conchospore release at a very low density, we added only one sporangial filament (\sim 70–150 μm) to each well in a 48-well plate under different light intensities (10, 40, and 80 $\mu\text{mol photons m}^{-2} \text{s}^{-1}$). Each well contained 1 mL PES medium without antibiotics and the sporangial filaments were cultured in a daily cooling system as described above. The number of wells in which conchospore release was observed was counted every 3 days over a 15-day culture period.

When culture density reached 100 fragments/mL, kanamycin (400 mg/L) was added to the PES medium to promote the release of conchospores. Using a 48-well plate with 1 mL medium to perform the experiment, six light intensities were used, which were 10, 20, 40, 60, 80, and 100 $\mu\text{mol photons m}^{-2} \text{s}^{-1}$. To calculate the rate of conchospore release, we first counted the total number of individual sporangial filament fragments in each well and then counted the number of those filaments which released conchospores. The count of conchospore-released filaments was performed every 3 days over a 15-day culture period. Each experiment was performed in triplicate and the error of data was standard deviation.

Morphological observations of sporangial filaments

In order to observe the morphological changes of sporangial filaments, from hollow cells to bipartite cells, light optical microscopy and TEM were conducted. Optical microscope observations were conducted using an inverted microscope (Nikon). For TEM observations, the material of the hollow cells was collected from high-density cultures (more than 13,000 fragments/mL) and the material of bipartite cells was collected from low-density cultures (~500 fragments/mL) after 3–11 days of culture. All material was cultured in the daily cooling system under a light intensity of $10 \mu\text{mol photons m}^{-2}\text{s}^{-1}$. Once the material was collected, samples were pre-fixed in 3% glutaraldehyde in sterilized natural seawater at pH 8.0–8.2 and then stored at 4 °C. When all of the samples were collected, they were post-fixed in 1% osmium tetroxide then dehydrated in ethanol, embedded in SPI-PON 812 (Spi-Chem Inc. West Chester, PA, USA), and trimmed. Ultrathin sections were obtained using an ultramicrotome EM UC7 (Leica Microsystems Ltd, Wetzlar, Germany), and the sections were observed by using HT7700 (Hitachi, Tokyo, Japan).

Culture and collection of sporangial filaments for transcriptome analysis

In order to explore the mechanism of the influence of culture density and light intensity on sporangial filaments at the gene expression level, we set up three groups, HD (for exploring the effect of high density and low light intensity), LD (for exploring the effect of low density and low light intensity) and HL (for exploring the effect of low density and high light intensity), to conduct transcriptome analysis. For the HD group, we put 50 mg (fresh weight) of cut-off sporangial filaments into 50 mL culture medium (final culture density of approximately 13,000 fragments/mL). For the LD group, we put 50 mg (fresh weight) of cut-off sporangial filaments into 5 L of culture medium (final density of approximately 130 fragments/mL). For the HL group, we put 50 mg (fresh weight) of cut-off sporangial filaments into 5 L culture medium (final density of approximately 130 fragments/mL). The light intensity of HD and LD was adjusted to $10 \mu\text{mol photons m}^{-2} \text{s}^{-1}$ and the light intensity of HL was adjusted to $80 \mu\text{mol photons m}^{-2}\text{s}^{-1}$. The sporangial filaments were cultured in PES medium with 400 mg/L kanamycin. All three groups were set up in triplicate and cultured in the daily cooling system as above and the flasks were shaken three times every day. The material was collected on the sixth day and frozen in liquid nitrogen then stored at -80°C for RNA extraction.

RNA extraction, library construction, and sequencing

Total RNA was extracted using the RNeasy Pure Plant Kit (Qiagen, Beijing, China) according to the manufacturer's instructions. Then, each RNA sample was analyzed by 1% agarose gel electrophoresis, and the quality and concentration of the RNA were evaluated using a NanoPhotometer[®] spectrophotometer (Implen, Munich, Germany), and an RNA Nano 6000 Assay Kit on the Agilent Bioanalyzer 2100 system (Agilent Technologies, Santa Clara, CA, USA), respectively. A total amount of 1.5 μg RNA per sample was used as input material. Libraries were constructed using nine samples which the quality test results reported were all grade A (highest grade for cDNA library construction). Illumina sequencing was performed by Beijing Novogene Bioinformatics Technology Co., Ltd. (Beijing, China).

Sequence reads quality control, transcriptome assembly, and annotation

The error rate, Q20 (percentage of bases with a Phred value > 20), Q30 (percentage of bases with a Phred value > 30), and GC-content were calculated. Clean reads, which were used for subsequent analysis, were obtained by removing reads containing adapter, ambiguous characters (N), and low-quality reads (50% bases with quality score $[?]20$). Filtered reads from all nine samples were used in the assembly using Trinity (Grabherr et al. 2011) to generate the reference transcriptome. The longest transcript of each gene was selected as the unigene. The length distributions of transcripts and unigenes were calculated. Sample alignment was conducted using RSEM (Li & Dewey, 2011). Gene function was annotated based on the following databases: the NCBI non-redundant protein sequences (Nr), NCBI non-redundant nucleotide sequences (Nt), Kyoto Encyclopedia of Genes and Genomes (KEGG), Gene Ontology (GO), Pfam, Clusters of euKaryotic Orthologous Groups of proteins (KOG), and Swiss-Prot.

Differentially-expressed gene analysis.

Differentially-expressed gene (DEG) analysis of three groups (three biological replicates per group) was performed using the DESeq2 R package (1.18.0) (Love, Huber, & Anders, 2014). DESeq provides statistical routines for determining differential expression in digital gene expression data using a model based on negative binomial distribution. The resulting P -values were adjusted using the Benjamini and Hochberg's approach for controlling false discovery rate. Genes with an adjusted P -value (padj) < 0.05 and $|\log_2(\text{FoldChange})| > 1$ were determined to be DEGs. Functional enrichment analysis of DEGs was performed using GO and KEGG. GO enrichment analysis was implemented by the Goseq R package, in which gene length bias was corrected (Young, Wakefield, Smyth, & Oshlack, 2010). GO terms with corrected P -values less than 0.05 were considered significantly enriched by DEGs. Pathway enrichment of DEGs was conducted by KOBAS software (Mao, Cai, Olyarchuk, & Wei, 2005) in KEGG, a database resource for understanding high-level functions and utilities of the biological system.

Gene set enrichment analysis in the KEGG database

In order to comprehensively judge the up- or down-regulated level of pathways in the two comparison groups, gene set enrichment analysis (GSEA) in KEGG was selected. GSEA is a computational method that determines whether an *a priori* defined set of genes shows statistically significant, concordant differences between two biological states (e.g. phenotypes). The GSEA based in the KEGG database was used according to the guidance of the accompanying online software, from the website: <http://software.broadinstitute.org/gsea/index.jsp>. The threshold to judge the significance of an enriched pathway is a q -value of false discovery rate (FDR q -value) $< 25\%$.

Validation of RNA-Seq data

Based on the annotated function, eight genes were used for validation by quantitative real-time polymerase chain reaction (qRT-PCR). For the internal controls, eIF4A was selected (Kong, Cao, Sun, Liu, & Mao, 2015). The information concerning the DEGs and qRT-PCR primers which were designed using Primer 5.0 software is listed in Suppl. Table. 1. The qRT-PCR was performed using an iQTM5 Multicolor Real-Time PCR Detection System (Bio-Rad, Hercules, CA, USA) with Fast Start Essential DNA Green Master (Roche, Basel, Switzerland). The qRT-PCR mix for one 20 μL reaction contained the following components: 5 μL of cDNA template, 10 μL of $2\times$ SYBR Green Master Mix, 1 μL of each primer (10 $\mu\text{mol}/\mu\text{L}$), and 3 μL of RNase-free water. The program was set as follows: 95 $^\circ\text{C}$ for 10 min, followed by 40 cycles of 95 $^\circ\text{C}$ for 10 s, 58 $^\circ\text{C}$ for 15 s and 72 $^\circ\text{C}$ for 25 s, then 61 cycles of 65 $^\circ\text{C}$ for 30 s. A qRT-PCR was conducted for each gene with three technical replicates of three biological replicates. Melting curve analysis was performed to confirm product specificity. The related gene expression values were calculated by the $2^{-\text{Ct}}$ method (Livak & Schmittgen, 2001).

Results

Effects of density and light intensity on sporangial filaments

The formation of bipartite cells by sporangial filaments under different densities and light intensities was analyzed (Fig. 1A), in which a high rate of formation ($> 80\%$) occurred at low density ([?] 1,000 fragments/mL) while in some cases no bipartite cells formed under high culture density (5,000–10,000 fragments/mL). From the time-line, 6–9 days was the peak period of formation and existence of bipartite cells at low density. According to the light intensity level, bipartite cells both formed and disappeared earlier in the groups under high light intensity ([?] 40 $\mu\text{mol photons m}^{-2}\text{s}^{-1}$), with high light intensity showing a promotion of bipartite cell formation. In addition, over the whole 15 days of observation, there was virtually no conchospore release in groups at different culture densities, with the exception of the random release of some conchospores in the group with 50 fragments/mL under 10–20 $\mu\text{mol photons m}^{-2}\text{s}^{-1}$ (data not shown).

As for conchospore release, at a density of 1 fragment/mL, almost all single sporangial filaments would release conchospores under low light intensity (10 $\mu\text{mol photons m}^{-2}\text{s}^{-1}$), but when light intensity reached 80 $\mu\text{mol photons m}^{-2}\text{s}^{-1}$, only about 33% of total single sporangial filaments released conchospores (Table 1). A similar inhibitory effect of high light on conchospore release was also observed at a density of 100

fragments/mL (Fig. 1B). Even though light intensity was subsequently reduced (from 40 $\mu\text{mol photons m}^{-2}\text{s}^{-1}$ to 10 or 0 $\mu\text{mol photons m}^{-2}\text{s}^{-1}$) on the fourth day, the inhibitory effect of light could not be eliminated (Fig. 1C). This meant that the inhibitory effect of high light on conchospore release was irreversible. Moreover, for growth of sporangial filaments, the fresh weight increased as light intensity increased in the range of 10–80 $\mu\text{mol photons m}^{-2} \text{s}^{-1}$ (Fig. 1D).

These results show that bipartite cells only formed under low density and the effect of light on sporangial filaments was multifaceted. On the one hand, high light accelerated the formation of bipartite cells and promote the growth of sporangial filaments, while on the other hand, conchospore release was inhibited by high light.

Morphological changes under different conditions of sporangial filaments

Based on the results of bipartite cell formation and conchospore release, the morphological changes of sporangial filaments are summarized (Fig. 2). When cultured at high density, sporangial filaments would retain their typical hollow form (Fig. 2B, E). When cultured at low density, approximately spherical and compact bipartite cells (Fig. 2C, F) would form from hollow cells, and that was the sign that sporangial filaments had reached maturity and were ready for conchospore release. When the conditions were suitable, such as low light, the mature bipartite cells would be released from the ridge structures one by one (Fig. 2F) and the released cells were conchospores (Fig. 2H). If the sporangial filaments were placed in complete darkness, conchospores were still released, but they were green in color and died (Fig. 2G). If the bipartite cells did not move and release, the sporangial filaments would elongate and branch (Fig. 2D), and finally became hollow cells again (Fig. 2E).

Ultrastructural characteristics of hollow cells and bipartite cells

In the hollow cells of sporangial filaments at high density, endoplasmic reticulum (Fig. 3A, B, G) and peripheral chloroplasts (Fig. 3A, F) were very developed. The cell wall of sporangial filaments was composed of an external pectin layer and an internal fiber layer (Fig. 3H) and some floridean starches were formed in hollow cells. A large vacuole was observed in the center of hollow cells (Fig. 3C, E, F) as well as structures suspected of being involved in formation of autophagosomes (Fig. 3B), fully-formed double-membrane coated autophagosomes (Fig. 3D) and vacuoles with a double membrane after autophagosome degradation (Fig. 3C, D, E, F). These observations showed that the formation and degradation of autophagosomes were the main causes of hollow cell formation of sporangial filaments at high density.

In sporangial filaments at low density, two semicircular cells formed typical bipartite cells with a large nucleus, many floridean starches and no vacuole (Fig. 4A, B, D). There were no pit connections or cell walls in the initial bipartite cells (Fig. 4A, B), but those formed when the two semicircular cells became two almost circular cells (Fig. 4D). As time went by, bipartite cells would become longer (Fig. 4C, E), vacuoles would reappear (Fig. 4C, E, F) and the number of autophagosomes would increase again (Fig. 4F). Finally, the bipartite cells entered into a vegetative growth form (Fig. 4E), like that observed under a light microscope (Fig. 2D). In addition, the tip cells of sporangial filaments at low density always retained their hollow form, in which only rough endoplasmic reticulum, chloroplasts and large vacuoles were left (Fig. 4G, H).

Transcriptome analysis of sporangial filaments

In order to explore the influence of light and density on sporangial filaments at the gene expression level, we set up three groups: HD (high culture density under low light intensity; more than 13,000 fragments/mL under 10 $\mu\text{mol photons m}^{-2} \text{s}^{-1}$, in which most cells were in the hollow form), LD (low culture density under low light; less than 150 fragments/mL under 10 $\mu\text{mol photons m}^{-2} \text{s}^{-1}$, in which bipartite cells would be formed and conchospores could be released) and HL (low culture density under high light intensity; less than 150 fragments/mL under 80 $\mu\text{mol photons m}^{-2} \text{s}^{-1}$, in which bipartite cell formation was promoted and conchospore release was inhibited) and performed transcriptome analysis.

Basic information of transcriptome data

A total of 602,683,400 raw reads was obtained through Illumina sequencing (Table 2). After filtering, 579,432,658 clean reads were obtained with a GC content around 65-66%. After assembly, 108,936 transcripts with a mean length of 1,344 bp and N50 value of 2,090 bp were obtained. Among these, 66,678 unigenes (the longest transcript of each gene) with a mean length of 1,287 bp and N50 value of 1,966 bp were selected as the reference transcriptome for subsequent analysis (Fig. 5).

Annotation of unigenes

For annotation of 66,678 unigenes, seven databases (NR, NT, KO, SwissProt, PFAM, GO, and KOG) were selected for annotation (Table 3). Of the total 66,678 unigenes, 48,189 (72.27%) were annotated in at least one database and 3,465 (5.19%) were annotated in all databases. In the GO database, the 40,351 unigenes were classified into three first-level terms (biological process, cellular component, and molecular function) and 56 second-level terms, among which the top terms of biological process, cellular component, and molecular function were cellular process, cell/cell part, and binding, respectively (Suppl. Fig. 2). The 12,133 annotated unigenes in KEGG were classified into nineteen categories in the second hierarchy, in which “translation”, “folding, sorting and degradation” and “carbohydrate metabolism” were the top three categories in the second hierarchy (Suppl. Fig. 3). The 16,639 unigenes annotated in KOG were classified into 26 categories, in which the top three categories were “general function prediction only”, “posttranslational modification, protein turnover, chaperones”, and “signal transduction mechanisms” (Suppl. Fig. 4).

Screening and clustering of differentially-expressed genes

The clean reads of nine samples were mapped to the assembled transcriptome and each mapped rate reached 85-88% (Table 2). In order to perform a comparative analysis, two comparative groups (HDvsLD, HLvsLD) were created to obtain DEGs with the screening conditions of q -value (p -adj) < 0.05 and $|\log_2(\text{Fold change})| > 1$. In HDvsLD comparison group, there were 3,322 DEGs with 1,738 up-regulated genes and 1,584 down-regulated genes, while in HLvsLD comparison group, there were 9,084 DEGs with 1,438 up-regulated genes and 7,646 down-regulated genes (Fig. 6). The Venn diagram showed that there were 1,221 DEGs which were found in both two comparison groups (Fig. 7). After using all 11,185 DEGs to make a heatmap cluster of nine samples, the result showed that the gene expression pattern of HD samples was closer to LD compared to HL samples, which indicated that the effects of light intensity were greater than those of culture density on gene expression levels (Fig. 8).

Validation of DEGs by qRT-PCR

In order to confirm the reliability of expression profiles based on RNA-Seq data, qRT-PCR experiments were conducted. We chose eight DEGs with high fragments per kilobase of exon model per million reads mapped (FPKM) values from 1,221 DEGs in both the comparison groups of HDvsLD and HLvsLD to perform the validation. Among them, five DEGs were down-regulated in HDvsLD and up-regulated in HLvsLD and another three DEGs were up-regulated in both HDvsLD and HLvsLD (Suppl. Table. 1). The results of qRT-PCR (Fig. 9) showed the up/down trend of all eight DEGs, when comparing the HD group with the LD group, were basically the same as the results of RNA-Seq. When comparing the HL group with the LD group, six genes were up-regulated and the expression of another two was close to that in the LD group. These results showed that the results of RNA-Seq were believable.

GO enrichment analysis of DEGs in HDvsLD and HLvsLD

Information regarding the top 10 enriched GO accession of DEGs is shown in Suppl. Table 2, in which besides ribosome-related GO accession, the GO accession of “small GTPase mediated signal transduction”, “regulated of GTPase activity”, “guanyl-nucleotide exchange factor activity”, “ribonucleoprotein complex biogenesis”, “intracellular signal transduction”, “regulation of hydrolase activity”, and “regulation of catalytic activity” were up-regulated in HDvsLD and down-regulated in HLvsLD. There was no significantly enriched accession (corrected P value > 0.05) among the down-regulated DEGs of the HDvsLD comparison group. Among the up-regulated DEGs of the HLvsLD comparison group, the top enriched GO accessions were “oxidoreductase activity”, “oxoacid metabolic process”, “organic acid metabolic process”, “carboxylic

acid metabolic process”, and “oxidation-reduction process”. In addition, the directed acyclic graph of biological processes showed that accessions related to GTPase were the most significantly enriched bottom GO terms among up-regulated DEGs of HDvsLD comparison group and down-regulated DEGs of HLvsLD comparison group (Suppl. Fig. 5, 6). These results showed that DEGs related to GTPase-mediated signal transduction played an important role in bipartite cell formation, and most of them were up-regulated in HDvsLD and down-regulated in HLvsLD.

KEGG enrichment of DEGs

Among all DEGs in the HDvsLD and HLvsLD comparison groups, there were a total of 105 enriched specific pathways in the KEGG database, which could be classified into eighteen categories in the second hierarchy. The number of up- and down-regulated DEGs in the two comparison groups of every pathway are shown in Suppl. Table. 3. In HDvsLD, there were more up-regulated DEGs than down-regulated DEGs in most pathways, but the opposite was observed in the HLvsLD comparison group, with far fewer up-regulated DEGs than down-regulated DEGs in most pathways, with the exception of some pathways related to energy accumulation. Among the top ten enriched pathways of DEGs (Suppl. Table. 4), pathways related to transport and catabolism, such as “Phagosome” and “Regulation of autophagy” were present in both the HDvsLD (up-regulated DEGs) and HLvsLD (down-regulated DEGs) groups, and the pathways related to energy accumulation, such as “carbon fixation in photosynthetic organisms”, “porphyrin and chlorophyll metabolism”, and “nitrogen metabolism” were present in the HLvsLD group (up-regulated DEGs).

Results of GSEA in KEGG

In order to comprehensively judge the up- or down-regulated level of pathways in the two comparison groups, GSEA in KEGG was conducted. The results of GSEA (Suppl. Table. 5) showed that, in the HDvsLD comparison group, 79 pathways were up-regulated, among which 40 pathways were significantly up-regulated (FDR q -value $< 25\%$) and five pathways were down-regulated, but of these, only one pathway (terpenoid backbone biosynthesis) was significantly down-regulated. In HLvsLD comparison group, there were a total of 58 up-regulated pathways, of which 47 pathways were significantly up-regulated, and 26 down-regulated pathways, of which six were significantly down-regulated. When comparing high density with low density (HDvsLD comparison group), most pathways were up-regulated significantly. This meant that down-regulation of some pathways led to the formation of bipartite cells under low density. From this point of view, those negative regulatory pathways of bipartite cell formation should also be down-regulated in HLvsLD comparison group, because bipartite cell formation was promoted by high light. The main pathways that met these conditions contained “ribosome”, “phagosome”, “endocytosis”, “regulation of autophagy”, and “phosphatidylinositol signaling system”. In addition, when focusing on light inhibition of conchospore release, energy accumulation-related pathways, such as “carbon fixation in photosynthetic organisms”, “porphyrin and chlorophyll metabolism”, “photosynthesis”, and “nitrogen metabolism” were up-regulated in HLvsLD comparison group. The results of GSEA were basically consistent with the results of DEG enrichment in KEGG, and supported the high credibility of the three transcriptomes.

Candidate key pathways and DEGs related to bipartite cell formation

Based on the above pathway analysis, we picked out a total of 404 DEGs which were present in both the up-regulated DEGs of the HDvsLD comparison group and the down-regulated DEGs of HLvsLD (data not shown). Using these 404 DEGs to perform KEGG enrichment, finally, five significantly-enriched pathways (q -value < 0.05) were obtained, which were “regulation of autophagy”, “inositol phosphate metabolism”, “phagosome”, “plant hormone signal transduction”, and “endocytosis” (Fig. 10, Table 4). In plants, phagocytosis of large particles, such as microbes, is always also described as endocytosis (Leborgne-Castel, Adam, & Bouhidel, 2010). Later, the “endocytosis” included both phagosome (ko04145) and endocytosis (ko04144). The key DEGs in inositol phosphate metabolism were all involved in phosphatidylinositol (PtdIns) metabolism. Interestingly, endocytosis, autophagy and PtdIns metabolism all play basic roles in adapting to changes in the environment and the differences in light and density could cause changes in the growth environment of sporangial filaments. Hence, the three associated environmental adaptive responses

were finally chosen as the key negative regulatory pathways of bipartite cell formation from hollow cells in *P. yezoensis*. Among the 404 DEGs, there were a total of 21 DEGs enriched in the three pathways (Suppl. Table. 6) and a sketch map of some DEGs in the three pathways is shown in Suppl. Fig. 7 and described as follows:

In PtdIns metabolism, phosphatidylinositol 3-kinase (PI3K or VPS34) mediates the phosphorylation of PtdIns to form PtdIns(3)P and myotubularin-related protein 1/2 mediates the resynthesis of PtdIns from PtdIns(3)P. Phosphatidylinositol 4-phosphate 5 kinase (PIP5K) and PTEN protein mediate PtdIns(4,5)P₂ formation from PtdIns(4)P and PtdIns(3,4,5)P₃, respectively.

In autophagy, autophagy-like protein 1 (ATG1 or ULK1) and PI3K stimulated the initial vesicle nucleation through the ULK complex and PI3K complex in the endoplasmic reticulum. AMP-activated protein kinase (AMPK) protein is an important upstream positive regulator, which stimulates autophagic processes by inhibiting the target of rapamycin pathway or by directly phosphorylating ULK1. ATG12 is a constituent gene of the ATG12-ATG5-ATG16 conjugate which stimulates membrane expression of the early autophagosome. Besides these four DEGs, there were many other DEGs annotated as ATGs (autophagy-related genes), which were only present in HDvsLD or HLvsLD, especially among the down-regulated DEGs of HLvsLD, such as ATG3, ATG4, ATG5, ATG7, and ATG8 (Suppl. Table. 7).

In endocytosis, PIP5K stimulates the initial formation of clathrin-coated vesicles on the plasma membrane. Rab proteins (belonging to the small GTPase protein family) play important roles in the aggregation and localization of transport vesicles. Among them, Rab5 and Rab8 mediate localization of the endosomal recycling compartment and the early endosome, Rab7 mediates localization of the late endosome and Rab11 mediates localization of the endosomal recycling compartment slowing recycling to the plasma membrane. In the early endosome, Ras-related C3 botulinum toxin substrate 1 (Rac1), which is stimulated by Rab5 and PI3K, activates NADPH oxidase. Another two DEGs, brefeldin A-inhibited guanine nucleotide-exchange protein and stromal membrane-associated protein, respectively, activate and inactivate Rab proteins. The importance of function related to GTPases was also confirmed in the results of DEG enrichment in the GO database (Suppl. Table. 2, Suppl. Fig. 5, 6).

Core-up regulated DEGs related to energy accumulation in HLvsLD

Both the results of DEGs and GSEA analysis of KEGG showed that the pathways related to energy accumulation were up-regulated in HLvsLD, including “porphyrin and chlorophyll metabolism”, “photosynthesis”, “carbon fixation in photosynthetic organisms”, “nitrogen metabolism” and “starch and sucrose metabolism”. We selected core-up regulated DEGs related to energy accumulation (Suppl. Table 8), which the DEGs were core enriched in GSEA and up-regulated in HLvsLD comparison group. The functions of these core up-regulated DEGs are:

In porphyrin and chlorophyll metabolism, glutamyl-tRNA reductase, glutamate-1-semialdehyde 2,1-aminomutase, hydroxymethylbilane synthase and oxygen-dependent protoporphyrinogen oxidase promote synthesis of protoporphyrin from glutamate. Magnesium chelatase subunit H, divinyl chlorophyllide a 8-vinyl-reductase and protochlorophyllide reductase promote chlorophyllide a (precursors of chlorophyll) synthesis from protoporphyrin. Finally, chlorophyll is synthesized by chlorophyll synthase.

In photosynthesis, three genes in photosystem II (photosystem II oxygen-evolving enhancer protein 1, photosystem II oxygen-evolving enhancer protein 2, photosystem II PsbU protein), the iron-sulfur subunit of cytochrome b6-f complex, and the gamma subunit of F-type H⁺-transporting ATPase were promoted by high light. In addition, light-harvesting complex I chlorophyll a/b binding protein 1 was also promoted. This indicates that photosynthesis would be promoted under high light.

Corresponding to the enhancement of chlorophyll synthesis and photosynthesis, carbon fixation was also greatly promoted under high light. There were 22 core up-regulated DEGs related to carbon fixation. In the C4 pathway, the key gene phosphoenolpyruvate carboxylase and another two genes, aspartate aminotransferase and malate dehydrogenase, promoted absorption of carbon dioxide. In the Calvin cycle, the core up-

regulated DEGs, fructose-1,6-bisphosphatase I (verified by qRT-PCR), fructose-bisphosphate aldolase-class I, fructose-bisphosphate aldolase, class II, glyceraldehyde 3-phosphate dehydrogenase, phosphoglycerate kinase (verified by qRT-PCR), ribose 5-phosphate isomerase A, ribulose-phosphate 3-epimerase, sedoheptulose-bisphosphatase and transketolase (verified by qRT-PCR) promoted the carbon fixation ability of sporangial filaments under high light. In addition, triosephosphate isomerase made the carbon fixation intermediate glyceraldehyde 3-phosphate form glycerone phosphate, which would then enter into the starch synthesis pathway.

In starch metabolism, 1,4-alpha-glucan branching enzyme promoted the formation of starch from amylose while starch phosphorylase promoted formation of D-Glucose 1-phosphate from starch. This meant that synthesis and consumption of starch were both promoted by high light.

In nitrogen metabolism, nitrate/nitrite transporter and nitrate reductase (verified by qRT-PCR) promoted extracellular nitrate absorption and intracellular nitrite formation. In addition, glutamine synthetase promoted glutamate synthesis which then entered into chlorophyll synthesis while carbonic anhydrase promoted the absorption of carbon dioxide which would enter into carbon fixation.

Those core-up regulated DEGs related to energy accumulation showed a much higher carbon fixation ability under high light and would promote vegetative growth of sporangial filaments, a hypothesis which was also proven in growth experiments (Fig. 1D).

Discussion

We found that free-living sporangial filaments had a very sensitive response to environmental conditions, and were influenced by culture density and light. TEM observation showed that autophagosome-like structures increased in hollow cells (formed under high density), disappeared in bipartite cells (formed under low density) and reappeared when bipartite cells entered into vegetative growth. Based on transcriptome analysis, three key environmental response pathways—autophagy, endocytosis and PtdIns metabolism—were significantly stimulated under high density and severely inhibited under bipartite cell-inducing conditions (low density, high light), showing how adaptation to different environments caused cyclical morphological changes, from hollow cells to bipartite cells, of free-living sporangial filaments. In addition, we also observed obvious promotion of vegetative growth which, due to the promotion of energy accumulation, was the main reason for the inhibition of conchospore release from bipartite cells under high light conditions in free-living sporangial filaments.

Environmental adaptation and morphological changes

High culture density causes multiple forms of cellular stress, such as nutrition starvation, hypoxia, increases in reactive oxygen species (ROS) and microbial infection. Compared with low density, many metabolic processes were activated under high density (Suppl. Table. 3, 5). Among them, three key essential responses (autophagy, endocytosis, PtdIns metabolism) to environmental changes were finally selected as the most important responses (Fig. 10, Table 4). Endocytosis is a process whereby the plasma membrane invaginates and pinches off, allowing extracellular particles or plasma membrane cargoes to enter the cell and mediate a plethora of cell biological processes such as the dispersal of signals within the cell, the turnover of plasma membrane necessary for cellular homeostasis, in concert with exocytosis, and the fight against pathogens (Battey, James, Greenland, & Brownlee, 1999; González-Gaitán, 2003; Leborgne-Castel et al., 2010; Lin & Guttman, 2010; Murphy, Padilla, Hasdemir, Cottrell, & Bunnett, 2009). Through numerous cell surface receptor-like kinases and related endocytic systems, plant cells are able to make a series of metabolic adjustments to adapt to changes in the external environment (Irani & Russinova, 2009). Among adaptive responses to environmental change, autophagy is the most important response to nutrient limitation under a high density of sporangial filaments. Autophagy is one of the key pathways that mediates stress-induced metabolic adaptation and damage control (Kroemer, Mariño, & Levine, 2010) and has been described in the model alga *Chlamydomonas reinhardtii* (Pérez-Pérez & Crespo, 2010). During autophagy, cytoplasmic components are non-selectively enclosed within a double-membrane vesicle known as the autophagosome and delivered to vacuoles for degradation of toxic components and recycling of needed nutrients (He & Klionsky,

2009; Liu & Bassham, 2012; Mizushima, Yoshimori, & Ohsumi, 2011; Pérez-Pérez, Lemaire, & Crespo, 2012). In this research, both the results of autophagosome-like structures observed by TEM and DEGs related to the autophagy pathway showed that the change to hollow cells under high density were caused by severe autophagy.

In both vesicle formation and the transport of the endocytic system and autophagy, genes related to PtdIns metabolism played important roles, especially the two key genes PI3K and PIP5K which catalyze the formation of PtdIns(3)P from PtdIns and PtdIns(4,5)P₂ from PtdIns(4)P. In *Chlamydomonas reinhardtii*, the inhibition and knockdown of PI3K led to significantly decreased cell growth, altered cell morphology, and higher lipid and starch contents (Ramanan et al., 2018). In this study, the number of starch structures in bipartite cells (formed under low density) was greater than that of hollow cells (formed under high density), while the expression of PI3K was down-regulated under low density (Fig. 3, 4, Suppl. Table. 6). PI3K also played an important role in the NADAPH oxidase activation process (Liu, Zhou, & Xing, 2012), through which ROS would be produced (Magnani & Mattevi, 2019), and ROS also is a stimulating factor of autophagy in algae (Pérez-Pérez et al., 2012). Another autophagy-inducing factor is AMPK (Kim, Kundu, Viollet, & Guan, 2011), which is stimulated when energy in cells is limited (Hardie, Ross, & Hawley, 2012). We found that the expression of AMPK was highest in the HD group and lowest in the HL group among the three groups. Correlated to the expression of AMPK, the expression of DEGs related to autophagy (such as ATG, ATG12, and PI3K) was also highest in HD and lowest in HL among the three groups (Suppl. Table. 6).

All these results are consistent with the results of the bipartite cell formation rate under different conditions of density and light intensity, which could indicate that bipartite cells are the adaptive morph in an environment with adequate nutrition, sufficient energy and low stress and in contrast, hollow cells are the adaptive morph in an environment of nutritional deficiency, energy deficiency and high stress. For subsequent studies of the development of sporangial filaments, the important candidate DEGs selected in this study, such as PI3K, PIP5K, ATG1, ATG12, Rab5, Rab7, and Rac1 (Suppl. Table. 6) are worth further in-depth study.

Vegetative growth and conchospore release

Conchospores could be seen as the intermediate between sporophyte and gametophyte. They are the seed sources of large-scale artificial culture of thallus of *Pyropia/Porphyra*. The mechanism of conchospore release from sporangial filaments has always been a mystery. Many studies showed that a relatively lower temperature, lower light intensity and shorter photoperiod were needed for the maturation and conchospore release of sporangial filaments (Chen, 1980; He & Yarish, 2006; Li et al., 2011; López-Vivas et al., 2015; Waaland et al., 1987). In this study, although high light (40–100 $\mu\text{mol photons m}^{-2} \text{s}^{-1}$) promoted the formation of bipartite cells (Fig. 1A) by inhibiting the pathways mentioned above, conchospore release was significantly inhibited by those light intensities of free-living sporangial filaments (Fig. 1B, C, Table. 1). In a study by Li *et al.* (Li et al., 2011), the free-living sporangial filaments of *P. yezoensis* grew fastest under appropriate high light (86 $\mu\text{mol photons m}^{-2} \text{s}^{-1}$). In our study, the results of analysis of both fresh weight (Fig. 1D) and gene expression changes under different light intensities also showed that high light (80 $\mu\text{mol photons m}^{-2} \text{s}^{-1}$) promoted the growth of sporangial filaments because of the promotion of a series of energy accumulation pathways, which included chlorophyll synthesis, photosynthesis, carbon fixation, absorption of nitrogen and starch synthesis (Suppl. Table. 3, 5, 8). From morphology, in the process via which bipartite cells enter into vegetative growth, bipartite cells would elongate with reappearance of the cell wall, pit connection structure, autophagosomes and small vacuoles (Fig. 4). When bipartite cells entered into vegetative growth, the stage of conchospore release would be skipped. It could be seen that the morphological change of sporangial filaments was a cyclical process (Fig. 2) and the bipartite cell stage was a special and short-term stage which appeared in low stress environments and the subsequent conchospore release of bipartite cells was a stage in competition with vegetative growth. Hence, the important steps in promoting conchospore release are: first, reducing the environmental pressure to promote formation of bipartite cells, and then keeping bipartite cells in a low vegetative growth environment, such as low light (10–20 $\mu\text{mol photons m}^{-2} \text{s}^{-1}$), to promote conchospore release.

Conclusion

We observed all the morphological changes caused by culture density and light intensity of free-living sporangial filaments through TEM and optical microscope visualization. The two important phenomena, bipartite cell formation and conchospore release, were detected. Through transcriptome analysis, we demonstrated that adaptive responses under different environments were the bases of morphological change in sporangial filaments of *P. yezoensis*. Further, conchospores released from bipartite cells need a low vegetative growth environment, such as low light. These results will be beneficial to fundamental research and production application of *P. yezoensis*.

Acknowledgments

The authors wish to acknowledge the financial support by the grant of Laboratory for Marine Biology and Biotechnology (OF2019NO07), Pilot National Laboratory for Marine Science and Technology (Qingdao), National Natural Science Foundations of China (41876160), National Key R&D Program of China (2018YFD0901500) and Ministry of Agriculture and Rural Affairs of the People's Republic of China (CARS-50).

Conflict of Interest

The authors declare no conflict of interest.

References

- Batley, N. H., James, N. C., Greenland, A. J., & Brownlee, C. (1999). Exocytosis and endocytosis. *The Plant Cell*, 11 (4), 643-659.
- Blouin, N. A., Brodie, J. A., Grossman, A. C., Xu, P., & Brawley, S. H. (2011). Porphyra: a marine crop shaped by stress. *Trends in plant science*, 16 (1), 29-37.
- Chen, G. (1980). Studies on the free conchocelis filament culture and seeding in *Porphyra haitanensis*. *Chin. J. Fish. Aquac.*, 4 (1), 19-29.
- Drew, K. M. (1949). Conchocelis-phase in the life-history of *Porphyra umbilicalis* (L.) Kütz. *Nature*, 164 (4174), 748.
- González-Gaitán, M. (2003). Signal dispersal and transduction through the endocytic pathway. *Nature reviews Molecular cell biology*, 4 (3), 213-224.
- Hardie, D. G., Ross, F. A., & Hawley, S. A. (2012). AMPK: a nutrient and energy sensor that maintains energy homeostasis. *Nature reviews Molecular cell biology*, 13 (4), 251-262.
- He, C., & Klionsky, D. J. (2009). Regulation mechanisms and signaling pathways of autophagy. *Annual review of genetics*, 43, 67-93.
- He, P., & Wu, W. (2003). Establishment and cultivation of cell line HB with high temperature resistance and fast growth in *Porphyra yezoensis*. *Shi yan sheng wu xue bao*, 36 (3), 191-196.
- He, P., & Yarish, C. (2006). The developmental regulation of mass cultures of free-living conchocelis for commercial net seeding of *Porphyra leucosticta* from Northeast America. *Aquaculture*, 257 (1-4), 373-381.
- Irani, N. G., & Russinova, E. (2009). Receptor endocytosis and signaling in plants. *Current opinion in plant biology*, 12 (6), 653-659.
- Kim, J., Kundu, M., Viollet, B., & Guan, K. (2011). AMPK and mTOR regulate autophagy through direct phosphorylation of Ulk1. *Nature cell biology*, 13 (2), 132-141.
- Kim, J. K., Yarish, C., Hwang, E. K., Park, M., & Kim, Y. (2017). Seaweed aquaculture: cultivation technologies, challenges and its ecosystem services. *Algae*, 32 (1), 1-13.

- Kong, F., Cao, M., Sun, P., Liu, W., & Mao, Y. (2015). Selection of reference genes for gene expression normalization in *Pyropia yezoensis* using quantitative real-time PCR. *Journal of applied phycology*, 27 (2), 1003-1010.
- Kroemer, G., Mariño, G., & Levine, B. (2010). Autophagy and the integrated stress response. *Molecular cell*, 40 (2), 280-293.
- Leborgne-Castel, N., Adam, T., & Bouhidel, K. (2010). Endocytosis in plant-microbe interactions. *Protoplasma*, 247 (3-4), 177-193.
- Li, B., & Dewey, C. N. (2011). RSEM: accurate transcript quantification from RNA-Seq data with or without a reference genome. *BMC bioinformatics*, 12 (1), 323.
- Li, X., Yang, L., & He, P. (2011). Formation and growth of free-living conchosporangia of *Porphyra yezoensis*: effects of photoperiod, temperature and light intensity. *Aquaculture Research*, 42 (8), 1079-1086.
- Lin, A. E.-J., & Guttman, J. A. (2010). Hijacking the endocytic machinery by microbial pathogens. *Protoplasma*, 244 (1-4), 75-90.
- Liu, J., Zhou, J., & Xing, D. (2012). Phosphatidylinositol 3-kinase plays a vital role in regulation of rice seed vigor via altering NADPH oxidase activity. *Plos One*, 7 (3).
- Liu, Y., & Bassham, D. C. (2012). Autophagy: pathways for self-eating in plant cells. *Annual review of plant biology*, 63 , 215-237.
- Livak, K. J., & Schmittgen, T. D. (2001). Analysis of relative gene expression data using real-time quantitative PCR and the 2- $\Delta\Delta$ CT method. *methods*, 25 (4), 402-408.
- López-Vivas, J. M., Riosmena-Rodríguez, R., Pacheco-Ruíz, I., & Yarish, C. (2015). Growth and reproductive responses of the conchocelis phase of *Pyropia hollenbergii* (Bangiales, Rhodophyta) to light and temperature. *Journal of applied phycology*, 27 (4), 1561-1570.
- Love, M. I., Huber, W., & Anders, S. (2014). Moderated estimation of fold change and dispersion for RNA-seq data with DESeq2. *Genome biology*, 15 (12), 550.
- Ma, Y., He, L., Huan, L., Lu, X., & Wang, G. (2019). Characterization of a high-growth-rate mutant strain of *Pyropia yezoensis* using physiology measurement and transcriptome analysis. *Journal of phycology* .
- Magnani, F., & Mattevi, A. (2019). Structure and mechanisms of ROS generation by NADPH oxidases. *Current opinion in structural biology*, 59 , 91-97.
- Mao, X., Cai, T., Olyarchuk, J. G., & Wei, L. (2005). Automated genome annotation and pathway identification using the KEGG Orthology (KO) as a controlled vocabulary. *Bioinformatics*, 21 (19), 3787-3793.
- Mizushima, N., Yoshimori, T., & Ohsumi, Y. (2011). The role of Atg proteins in autophagosome formation. *Annual review of cell and developmental biology*, 27 , 107-132.
- Murphy, J. E., Padilla, B. E., Hasdemir, B., Cottrell, G. S., & Bunnett, N. W. (2009). Endosomes: a legitimate platform for the signaling train. *Proceedings of the National Academy of Sciences*, 106 (42), 17615-17622.
- Perez-Perez, M. E., & Crespo, J. L. (2010). Autophagy in the model alga *Chlamydomonas reinhardtii* . *Autophagy*, 6 (4), 562-563.
- Perez-Perez, M. E., Lemaire, S. D., & Crespo, J. L. (2012). Reactive oxygen species and autophagy in plants and algae. *Plant Physiology*, 160 (1), 156-164.
- Provasoli, L. (1968) Media and prospects for the cultivation of marine algae. In: Watanabe A, Hattori A (eds.) Cultures and Collections of Algae. Proceedings of the U.S.-Japan Conference, Hakone, September. Japanese Society of Plant Physiologists, Tokyo. pp 63-75

Ramanan, R., Tran, Q.-G., Cho, D.-H., Jung, J.-E., Kim, B.-H., Shin, S.-Y., . . . Lee, S.-J. (2018). The ancient phosphatidylinositol 3-kinase signaling system is a master regulator of energy and carbon metabolism in algae. *Plant Physiology*, 177 (3), 1050-1065.

Sun, A., & Zheng, C. (1996). Preliminary report on suspension culture of clon of *Porphyra yezoensis* conchosporangial filaments in the production of conchospores for purple laver aquaculture. *Oceanologia et Limnologia Sinica*, 27 (6), 667-668.

Waaland, J. R., Dickson, L. G., & Carrier, J. E. (1987). Conchocelis growth and photoperiodic control of conchospore release in *Porphyra torta* (rhodophyta). *Journal of phycology*, 23 (3), 399-406.

Yang, L., & He, P. (2004). Effect of temperature, light intensity and conchosporangium density on conchospores releasing in *Porphyra yezoensis*. *Marine Ticheries*.

Yoji, N., Naobumi, S., Masahiro, K., Nobuhiko, O., Motoshige, Y., Yuya, S., . . . Atsumi, T. (2013). The First Symbiont-Free Genome Sequence of Marine Red Alga, Susabi-nori (*Pyropia yezoensis*). *Plos One*, 8 (3), e57122.

Young, M. D., Wakefield, M. J., Smyth, G. K., & Oshlack, A. (2010). Gene ontology analysis for RNA-seq: accounting for selection bias. *Genome biology*, 11 (2), R14.

Tables

Table 1 Conchospores release of single sporangial filament

Light Intensities ($\mu\text{mol photons m}^{-2} \text{ s}^{-1}$)	Released holes / total holes					Final Percentages (%)
	3 rd day	6 th day	9 th day	12 th day	15 th day	
10	0/48	43/48	47/48	47/48	47/48	97.91
40	0/48	12/48	37/48	40/48	40/48	83.33
80	0/48	1/48	5/48	16/48	16/48	33.33

Table 2 Sequence analysis summary of nine samples

Sample	Raw Reads	Clean Reads	Clean Bases (Gb)	Error (%)	Q20 (%)	Q30 (%)	GC Content (%)	Total Mapped
HD1	60,828,832	58,727,046	8.81	0.03	96.74	92.44	65.88	51,715,1 (88.06%)
HD2	74,995,026	72,275,946	10.84	0.03	96.73	92.41	66.08	63,689,8 (88.12%)
HD3	58,084,156	55,980,466	8.4	0.03	96.92	92.77	65.45	49,338,5 (88.14%)
HL1	86,950,532	83,286,642	12.49	0.03	96.35	91.79	66.68	73,023,1 (87.68%)
HL2	79,386,504	75,623,196	11.34	0.03	96.66	92.47	66.02	66,394,9 (87.80%)
HL3	89,235,100	86,216,082	12.93	0.03	96.58	92.22	65.12	73,591,0 (85.36%)
LD1	56,786,392	54,589,112	8.19	0.03	96.76	92.55	66.10	48,113,2 (88.14%)

Sample	Raw Reads	Clean Reads	Clean Bases (Gb)	Error (%)	Q20 (%)	Q30 (%)	GC Content (%)	Total Mapped
LD2	54,384,772	52,324,388	7.85	0.03	96.75	92.56	65.89	45,862,7
LD3	42,032,086	40,409,780	6.06	0.03	96.55	92.06	66.64	(87.65%) 35,528,6
Total	602,683,400	579,432,658	86.91					(87.92%)

Q20: Percentage of bases with a Phred value >20; Q30: Percentage of bases with a Phred value >30.

Table 3 Number of unigenes annotated in seven databases

Databases	Number of Unigenes	Percentage (%)
Annotated in NR	27,706	41.55
Annotated in NT	10,672	16.00
Annotated in KEGG	12,133	18.19
Annotated in SwissProt	28,356	42.52
Annotated in PFAM	40,351	60.51
Annotated in GO	40,351	60.51
Annotated in KOG	16,639	24.95
Annotated in all Databases	3,465	5.19
Annotated in at least one Database	48,189	72.27
Total Unigenes	66,678	100

Table 4 Significantly enriched pathways of selected 404 DEGs. Basis for DEG selection: a. up-regulated in HDvsLD comparison group; b. down-regulated in HLvsLD comparison group.

Pathway Terms	KEGG ID	Corrected P-Value	DEGs Number
Regulation of autophagy	ko04140	0.0001	7
Inositol phosphate metabolism	ko00562	0.0010	7
Phagosome	ko04145	0.0016	7
Plant hormone signal transduction	ko04075	0.0121	4
Endocytosis	ko04144	0.0121	8

Figure legends

Figure 1 Effects of culture density and light intensity on sporangial filaments. A: Effects of density and light on formation of bipartite cells (mean \pm s.d. of three repetitions); B: Effects of light on conchospores release at density of 100 fragments/mL (mean \pm s.d. of five repetitions); C: Effects of light reduction on conchospore release at density of 100 fragments/mL (mean \pm s.d. of six repetitions); D: Effects of light on fresh weight changes (mean \pm s.d. of three repetitions).

Figure 2 Morphological change cycle of sporangial filaments under different conditions. A: Conchocelis of *P. yezoensis*, white arrow showed a sporangial filament in conchocelis; BE: Typical hollow form of sporangial filaments; CF: Typical bipartite cells of sporangial filaments; D: Vegetative growth form of bipartite cells; G: Released conchospores under complete darkness condition; H: Normal releasing conchospores; I: Thallus of *P. yezoensis*; Bar in all figures were 20 μ m.

Figure 3 Ultrastructural characteristics of hollow cells of sporangial filaments. A: Early hollow cell; B: Forming autophagosome in endoplasmic reticulum (local enlargement of A); C: Late hollow cell; D: Formed double membrane coated autophagosome (local enlargement of C); E: A vacuole with double membrane after autophagosome degradation; F: A hollow cell with many vacuoles separated by double membrane; G: Details of nucleus and rough endoplasmic reticulum; H: Details of cell wall of sporangial filaments; Ch: chloroplast; As: autophagosome-like structure; RER: rough endoplasmic reticulum; SER: Smooth endoplasmic reticulum; V: Vacuole; P: Pyrenoid; FS: Floridean starch; N: Nucleus; CW: Cell wall; PL: Pectin layer; FL: Fibrous layer; Black arrow: Small vacuole formed by degradation of autophagosome-like structure; Black arrowhead: Double membrane structure of autophagosome-like structure; Bar: 500 nm (BE), 200 nm (D), 1 μ m (other figures).

Figure 4 Ultrastructural changes of bipartite cells. AB: Early bipartite cells; C: Initial elongation of bipartite cells; D: Late bipartite cells with cell wall and pit connection; E: Elongated cell with pit connection; F: Increased autophagosomes in elongated cell; GH: Tip cells of sporangial filaments under low density; Ch: chloroplast; As: Autophagosome-like structure; RER: Rough endoplasmic reticulum; V: Vacuole; P: Pyrenoid; FS: Floridean starch; N: Nucleus; Pc: Pit connection; Arrow: Cell wall; Arrowhead in E: Pit connection; Bar: 1 μ m in all figures.

Figure 5 Length distribution of transcripts and unigenes. N50 (90) length was defined as the length for which the collection of all contigs of that length or longer contains at least 50% (90%) of the total of the lengths of the contigs, and for which the collection of all contigs of that length or shorter contains at least 50% (90%) of the total of the lengths of the contigs.

Figure 6 Volcano maps of DEGs. Above the dotted line, the dots on the left (green) represent down-regulated DEGs ($p\text{-adj} < 0.05$ and $|\log_2\text{Fold change}| > 1$); the dots on the right (red) represent the up-regulated DEGs ($p\text{-adj} < 0.05$ and $|\log_2\text{Fold change}| > 1$).

Figure 7 Venn diagram of DEGs.

Figure 8 Heat map cluster of total 11,185 DEGs of nine samples. The Y axis represents relative expression, red color represents up-regulation and blue color represents down-regulation.

Figure 9 Results of qRT-PCR of eight DEGs in three groups. LD group was set as the control (mean \pm s.d. of three repetitions).

Figure 10 Pathways enriched of 404 DEGs. Basis for DEG selection: a. up-regulated in HDvsLD comparison group; b. down-regulated in HLvsLD comparison group.

Supporting information

Suppl. Table. 1 Information of DEGs and primers of qRT-PCR.

Suppl. Table. 2 Top ten GO enrichment accessions of DEGs.

Suppl. Table. 3 Number of up or down-regulated DEGs in every enriched pathway.

Suppl. Table. 4 Top ten enriched pathways in KEGG of DEGs.

Suppl. Table. 5 Gene Set Enrichment Analysis in KEGG.

Suppl. Table. 6 Information of key negative regulatory DEGs related to bipartite cells formation.

Suppl. Table. 7 Information of total DEGs enriched in autophagy pathway.

Suppl. Table 8 Information of core-up regulated DEGs related to energy accumulation in HLvsLD comparison group.

Suppl. Fig. 1 Linear prediction between number of filaments fragments and fresh weight.

Suppl. Fig. 2 Gene function classification of unigenes annotated by GO.

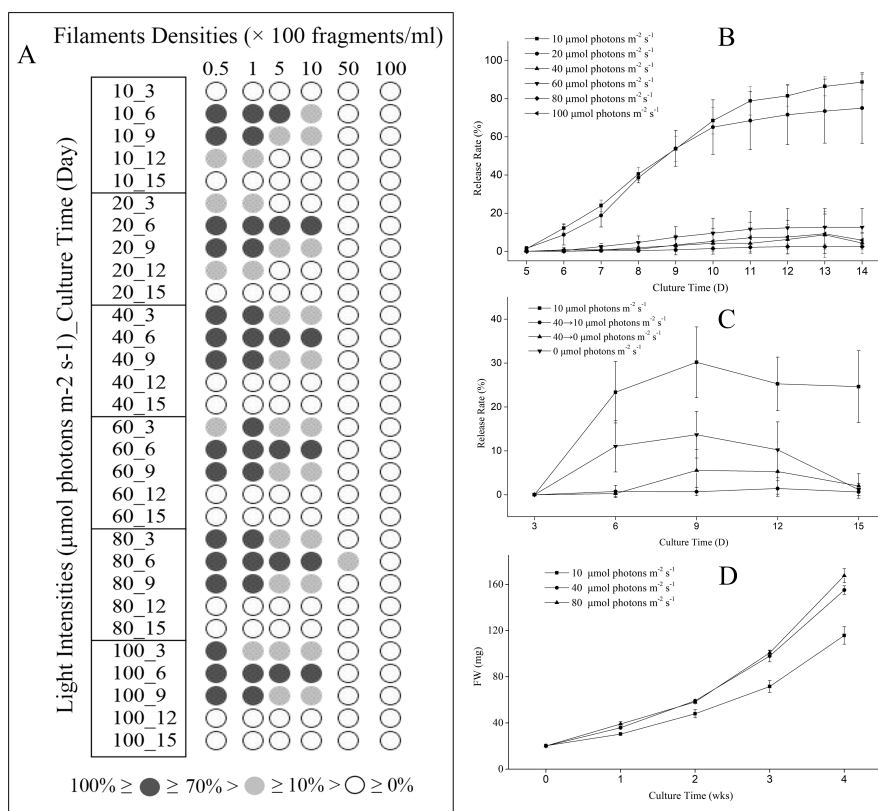
Suppl. Fig. 3 Gene function classification of unigenes annotated by KEGG.

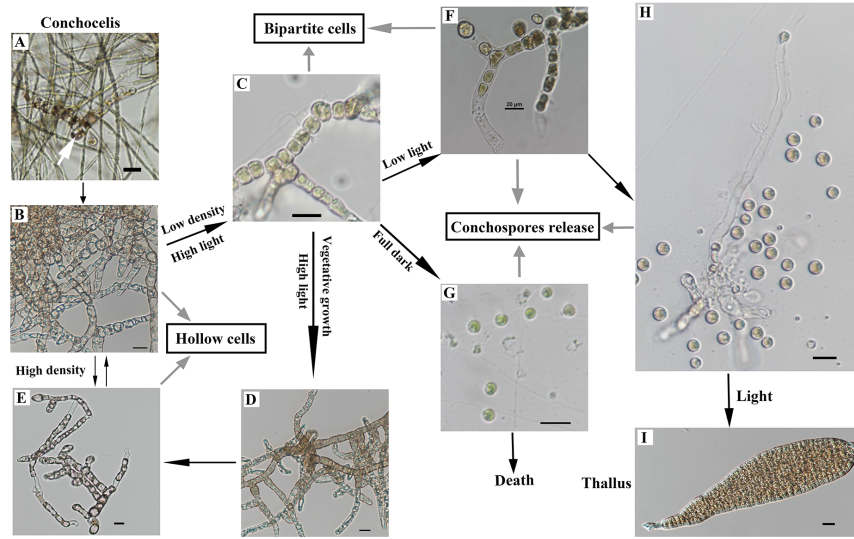
Suppl. Fig. 4 Gene functional classification of all unigenes annotated by KOG.

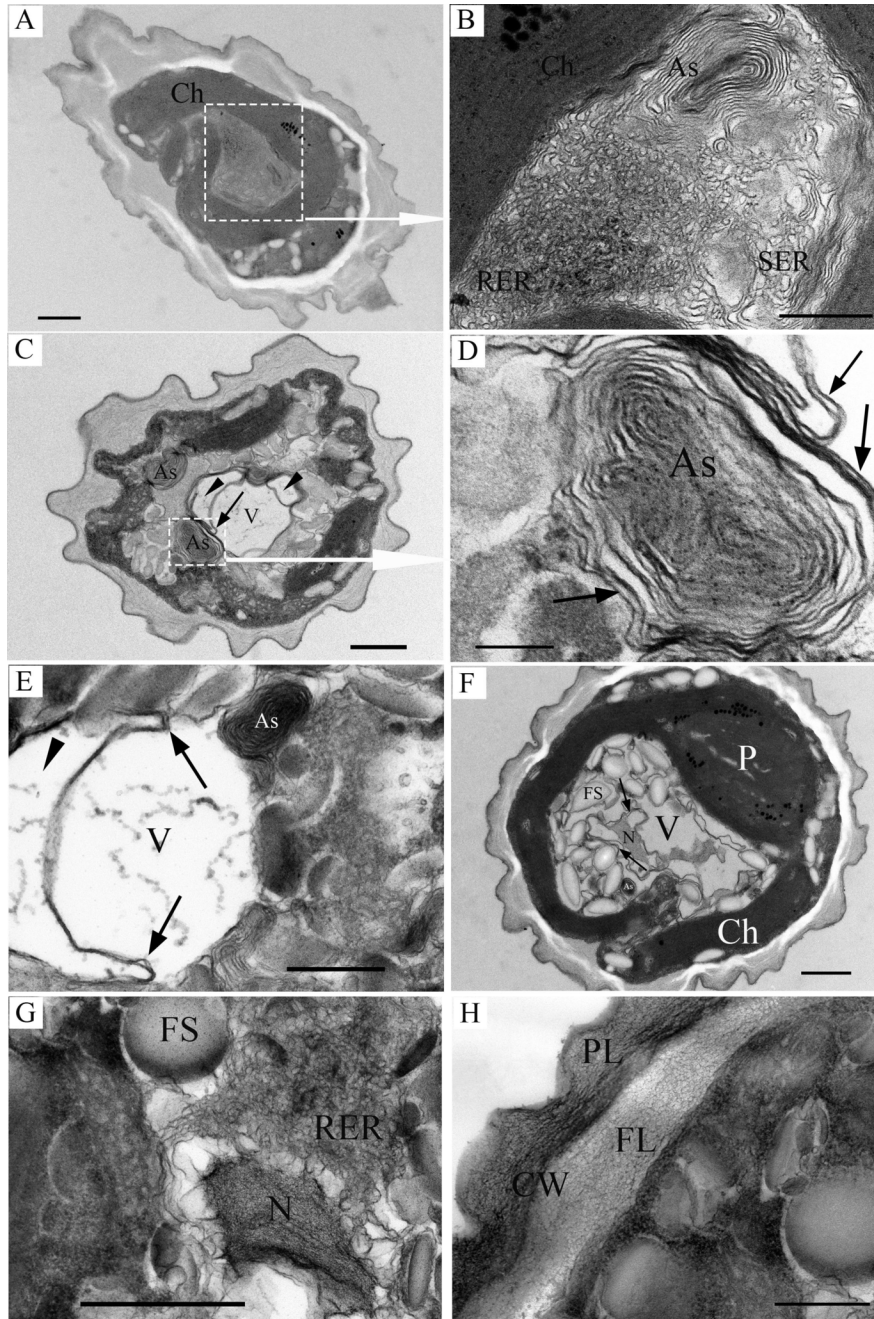
Suppl. Fig. 5 Directed acyclic graph of biological process in GO of up-regulated DEGs in HDvsLD comparison group.

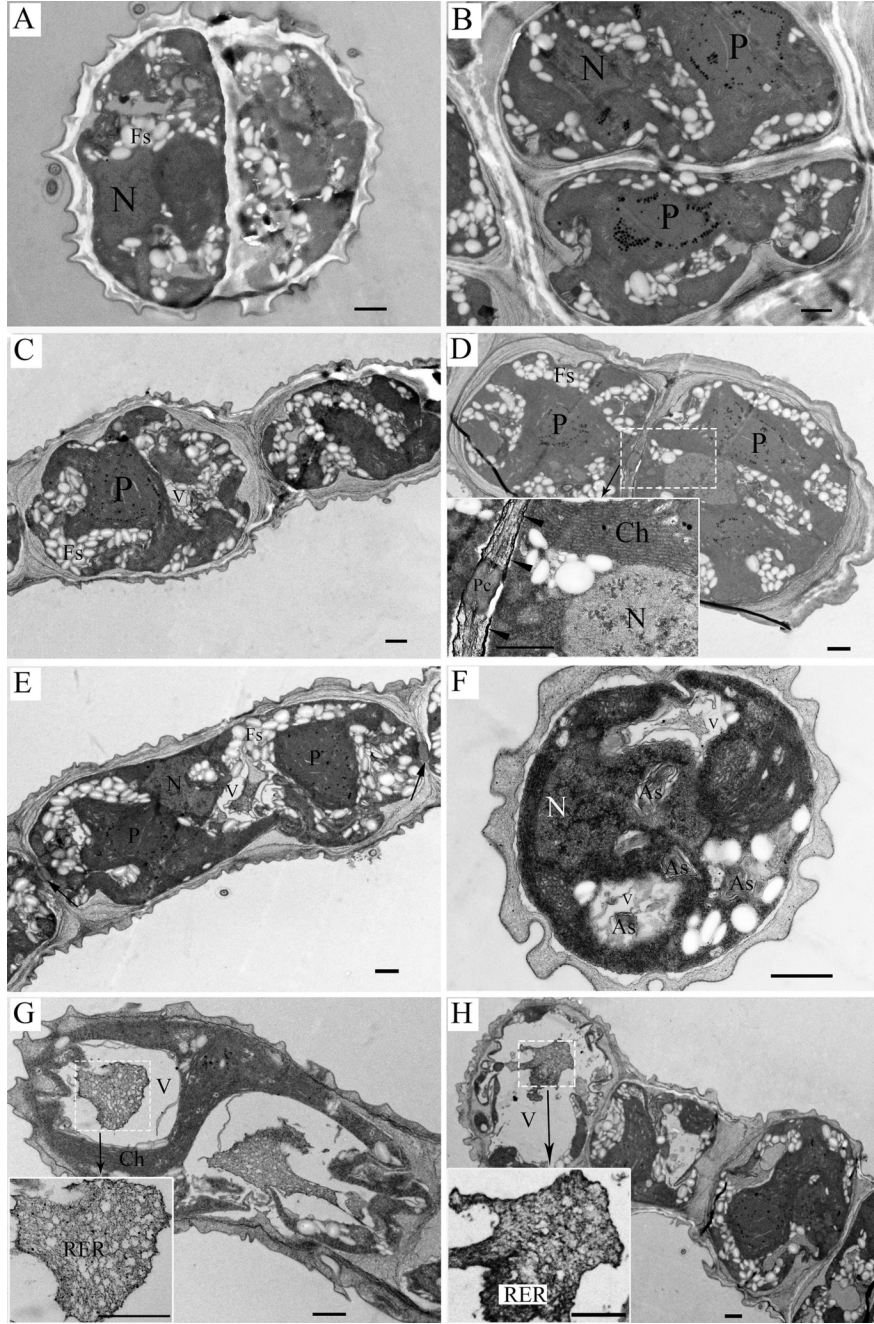
Suppl. Fig. 6 Directed acyclic graph of biological process in GO of down-regulated DEGs in HLvsLD comparison group.

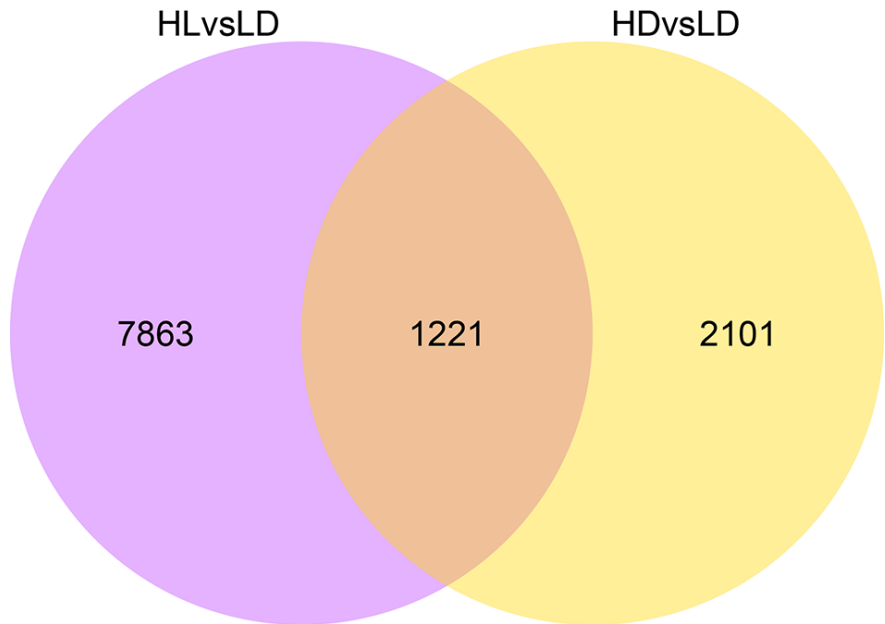
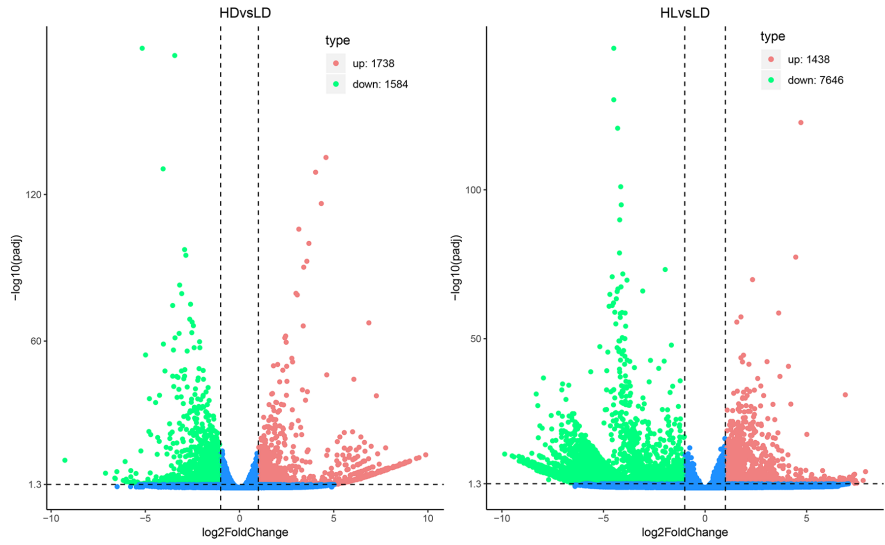
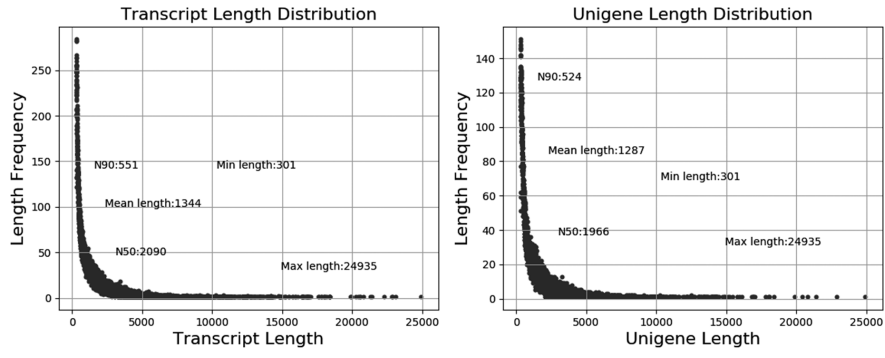
Suppl. Fig. 7 Sketch map of important DEGs in the three basic environmental adaptive responses.

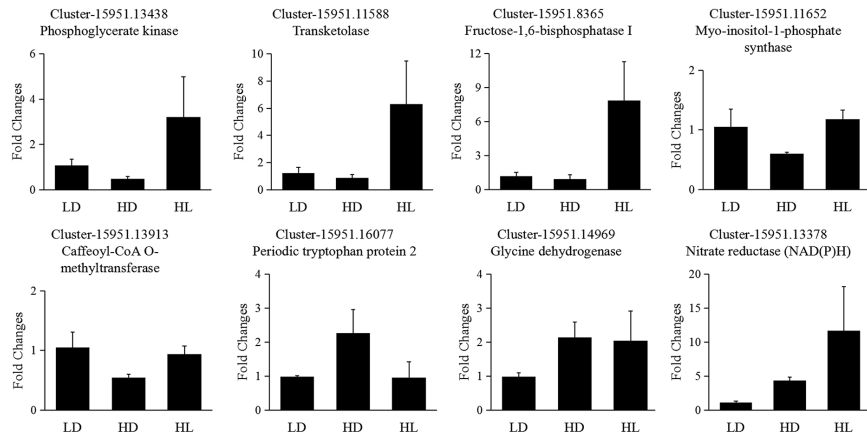
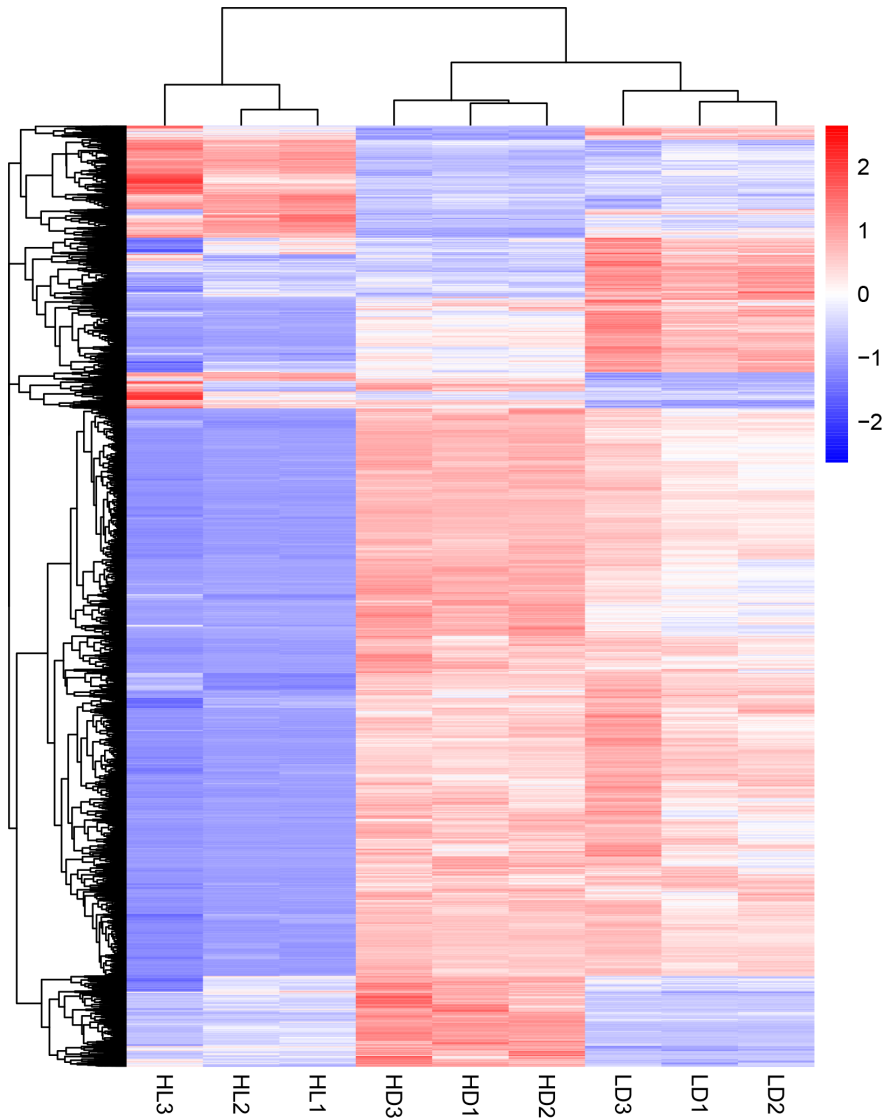












Statistics of Pathway Enrichment

